1998

X-Ray Spectroscopic Mapping of Three Unusual Active Galaxies (NGC 4258, NGC 1097, and NGC 1068)

Jeremy Kotter '98
Illinois Wesleyan University

X-ray Spectroscopic Mapping of Three Unusual Active Galaxies
(NGC 4258, NGC 1097, & NGC 1068)

Jeremy Kotter

Illinois Wesleyan University

Department of Physics

Bloomington, Illinois

April 22, 1998

1. Introduction

One enigmatic class of objects whose structures are interesting and only recently explored are active galactic nuclei (AGN). These are galaxies in which massive black holes sit at the center and accrete matter. The term "active" refers to energetic processes which are not directly attributable to stars and which occur in the innermost portions of galaxies. Astrophysicists have developed general descriptions of AGN, but details about these objects remain incomplete. Notably, the thermal and ionization structures of AGN accretion disks and the geometries of the circum-source clouds which surround the black hole and comprise an important portion of the energy emitting core, as well as the importance of thermal stability to the emission of radiation, is unclear at this time. Therefore, along with my research advisor, Dr. Cynthia Hess, I have studied the unusual active galaxies NGC 4258, NGC 1097, and NGC 1068 in an attempt to shed light upon the morphologies of their central regions.

AGN are very bright in their X-ray emission, often as much as 100,000 times as luminous as the Sun. The current model invoked to explain the enormous luminosity generated by AGN in such limited space is that of a "central engine": a supermassive black hole surrounded by a very hot "accretion disk" of inwardly-spiraling material. Accretion disks with temperatures reaching millions of Kelvin are a strong source of X-rays in AGN. In an accretion disk, matter falling toward the black hole gains kinetic energy, is stripped of some electrons, and subsequently releases energy through electromagnetic radiation. As photons move outward from the nucleus they pass through two different gaseous regions. The first is the "broad line region" (BLR) and the second is the "narrow line region" (NLR). The BLR does not exhibit any "forbidden lines" (i.e. transitions from metastable excited states) and therefore has an estimated density of

approximately 10^8 ions/cm^3 (such that the metastable states are collisionally de-excited and cannot form) (Zeilik *et. al.* 1992). The NLR does produce forbidden emission lines (i.e. it is less dense than the BLR), and it also contains significantly more dust then the BLR (leading some to consider the radius at which dust begins to redirect radiation significantly to be the line of demarcation between these two regions).

NGC 4258 is a very intriguing AGN with unusual attributes. It is known to exhibit maser activity in the region surrounding its warped accretion disk (Neufield & Maloney 1995), and it also emits jets of energetic radiation from its supermassive central black hole (~10^8 Mo) (Greenhill et al. 1995). The term "maser" stands for Microwave Amplification through Stimulated Emission of Radiation. Maser regions often occur near very large molecular clouds in AGN. In the case of NGC 4258 the masing molecule is H_2O. These regions of maser emission are extremely small on an astronomic scale (generally tens of astronomical units (AU)[1] across) and are very dense (5×10^6 ions/cm^3) as compared to the interstellar medium (Zeilik *et. al.* 1992). They are usually regarded as the signatures and locations of star formation. Maser activity results in intense, coherent light which is narrowly directed. It also creates unexpected molecular population inversion within AGN (i.e. the number of H_2O molecules in the upper energy levels is greater than the number in lower energy states).

The highly energetic jets (sometimes referred to as astrophysical jets) seen in NGC 4258 and other AGN are typically 180 degrees apart and tend to remain stable for lengths of thousands of parsecs[2] (Zeilik *et. al.* 1992). The jets are composed of electrons traveling near the speed of

---

[1] 1 AU is the mean distance between the Earth and the Sun.

[2] 1 parsec = 3.26 light years

light and produce synchrotron emission due to magnetic fields generated by the AGN.

The unusual geometry of NGC 4258 and the significant reprocessing (i.e. absorption and subsequent reemission of radiation) of the continuum and jets by its warped accretion disk make it an excellent object to study. NGC 1097 also exhibits the emission of energetic jets of plasma and radiation, while NGC 1068 exhibits maser activity. We hope to learn geometric information (e.g. volume and distance from the central engine) about the X-ray emitting gas within the AGN in unprecedented detail through spectroscopy and modeling of the thermal stability of the hot gas near the central engine.

A. X-ray Emission from AGN

One of the most important features of the spectrum of any AGN is its continuum. The "continuum" refers to the emission of the object over a continuous range of wavelengths. It is distinct in origin and appearance from the discrete spectral features whose specific energies are related to the energies of atomic transitions. The continuum is important because it is a direct probe of the ongoing processes near the black hole. In addition, an understanding of the continuum constrains the shape of the spectrum which irradiates the line emitting gas.

One frequently occurring continuum is a thermal continuum: the result of strong atomic interactions and motions which produce a great deal of energy (Peterson 1997). One such thermal spectrum is that of a "blackbody". A blackbody is an object which absorbs all incident electromagnetic radiation. In order for a blackbody to maintain thermal equilibrium it must emit radiation at the same rate at which it is absorbing. This is both an important and a common continuum component when studying the spectra of AGN.

Another important AGN continuum component is that produced by Compton scattering.

This occurs when photons are scattered by free electrons. Bremsstrahlung, or "braking radiation", is also an important process in understanding the continuum spectra of AGN. Thermal bremsstrahlung occurs when a free electron is accelerated by encountering a more massive object (such as a nucleus). Finally, the absorption and reemission of radiation by ambient hydrogen within the AGN contributes to the shape of the continuum spectrum emerging from the central engine.

The continuum spectra of AGN are know to be very complex, with X-rays accounting for approximately 10% of the total luminosity of the object (Zeilik *et. al.* 1992). There is a strong variability in the higher-energy region of the continuum. The long-term X-ray variability of AGN is on the order of days or weeks and seems to be correlated with changes in the optical and ultraviolet (UV) emission (Peterson 1997). However, AGN have been observed to exhibit periods of X-ray variability on the order of hours. This more rapid time variability seems to indicate that these X-rays are being emitted from very near the central engine, since the period of the fluctuations must be of the same order as the light travel time across the emitting medium. Therefore, an X-ray observation provides information about the innermost regions of an AGN.

Our approach is to use spectroscopy to probe the X-ray emitting gases in the AGN NGC 4258, NGC 1097, and NGC 1068. Spectroscopic observations yield new information about the physical processes in the AGN. Our work falls in the realm of high energy astrophysics, referring to our use of telescope observations of celestial objects in the X-ray region (0.1 - 100 keV) of the electromagnetic spectrum, where the radiation has higher energy than visible light. Typically, 0.1 - 2.0 keV is termed the "soft-X-ray" region, 2.0-100 keV is known as the "hard-X-ray" region, and radiation at energies over 100 keV is classified as gamma rays. Traditionally, the

boundary between soft and hard X-rays was set by instrumental considerations.

Spectroscopic observation provides a wealth of information about AGN. The relative strengths of emission lines can provide information about electron densities and temperatures in the gas. The presence of specific ions and their emission line widths can also be determined for any discrete feature from X-ray spectroscopy. Photon-particle interactions in the AGN (i.e. blackbody radiation, Compton scattering, bremsstrahlung, etc.) are also apparent from a fit of the continuum spectrum. Finally, the time variability of the AGN can be explored through spectroscopy. Flux and luminosity ratios can be calculated at different epochs within the variability cycle in order to provide information on the processes occurring near the central engine of the AGN.

B. The AGN

NGC 1068 is a relatively famous AGN, and it was one of the first of many to be discovered by the astronomer Carl Seyfert. It is a "Seyfert 2" galaxy which denotes that its emission lines are relatively narrower than those produced by "Seyfert 1" galaxies. Past X-ray observations of NGC 1068 have used a variety of instruments and have been focused upon many different analyses. Netzer *et. al.* (1993) used data from the Astro-1 and ROSAT satellites and focused upon the emission lines from highly ionized oxygen and iron K and L shell transitions (i.e. transitions into the n=1 and n=2 states respectively). They attributed the more highly ionized gases to regions closer to the nucleus and modeled various geometries for the X-ray emitting gases. They found that successful models required an underabundance of oxygen as well as an overabundance of iron. They then showed that optical and UV observations of the NLR are consistent with these deviations from cosmic abundances.

Ueno *et. al.* (1994) used ASCA data and reported strong emission lines from hydrogen- and helium-like ions of Ne, Mg, Si, S, along with lithium- and neon-like Fe. They also studied the structure of the hydrogen-like and helium-like Fe K line emission near 6.5 keV. They fit spectra from both hard and soft X-ray emission and determined a best fit continuum of the soft X-ray emission to be a combination of a power law model and bremsstrahlung. They then added successive narrow Gaussian emission lines to this continuum model until they saw no further improvement in the fit of their model and identified these discrete Gaussian features with known transitions from both highly ionized Fe and Ne ions. Their work supported the hypothesis of a strong starburst component along with a high column density which obscures the AGN. They propose detailed modeling in order to derive the physical parameters of NGC 1068.

NGC 1097 has also been widely studied across the electromagnetic spectrum from the infrared to the X-ray. Perez-Olea and Colina (1996) used *Einstein* and ROSAT satellite data. ROSAT was launched in 1990 and is a joint U.S., German, and U.K. satellite with modest instrument resolution. Perez-Olea and Colina calculated the ratio of the X-ray luminosity to the luminosity of the hydrogen Lyman-α transition in order to determine whether the X-ray emission from a circum-nuclear ring of NGC 1097 should be considered to be due to starbursts or to AGN activity. They found that luminosity ratio to be consistent with that of nearly edge-on starbursts.

X-ray observation of the nucleus of NGC 1097 was also undertaken in order to determine the source of previously unseen broad line emission from the galaxy. Storchi-Bergmann, Baldwin, and Wilson (1993) explored the X-ray continuum, finding it 'featureless', and speculate on the relationship between the broad line region and the optical jets which extend to a distance of tens of kiloparsecs from the nucleus. They find that an effective model accounting for the line profiles

is that of a biconical outflow of material, but they do not rule out the possibility of an elliptical accretion disk.

NGC 4258 is one of the nearest AGN. A study of the megamaser observations of NGC 4258 by Miyoshi and Greenhill (1995) showed that a massive black hole was present in the AGN. However, two years later Burbridge and Burbridge (1997) claimed that the ejection of gas from the nucleus proves that the ejection is coming from within a cone with an angle of less than 40° but that it does not necessarily provide evidence for a massive black hole.

We chose to study these three AGN because they exhibited unusual behavior which suggests interesting reprocessing of the enormous energies produced at their cores. In section 2 a detailed description of the instruments and methods used for data analysis is provided. The third section describes the technique and history of an analysis with thermal instability. Finally, our results and conclusions are presented in section 4.

2. Observations

ASCA, formerly named Astro-D, is a joint satellite mission between Japan and the United States. ASCA was launched on February 20, 1993. The telescope has four large-area X-ray telescopes. ASCA combines imaging capability with a broad bandpass, good spectral resolution, and a large effective area (http://heasarc.gsfc.nasa.gov/docs/asca/asca2.html). ASCA is the first X-ray astronomy mission to utilize Charge Coupled Devices (CCDs). A CCD is typically a silicon chip which consists of thousands of tiny pixels arranged in rows and columns. When an incident photon strikes an individual pixel it dislodges an electron, causing a net charge on the pixel. The primary scientific purpose of ASCA is "the X-ray spectroscopy of astrophysical plasmas-especially the analysis of discrete features such as emission lines and absorption edges." A Gas

Imaging Spectrometer (GIS) is at the focus of two of the telescopes, while a Solid-state Imaging Spectrometer (SIS) is at the focus of the other two. The GIS is a gas imaging scintillation proportional counter, while the SIS is a (CCD) camera. The SIS has an energy range from 0.4 keV to 10 keV, an energy resolution of 2 percent at 5.9 keV, and a field of view of 22 by 22 square arcminutes (http://heasarc.gsfc.nasa.gov/docs/asca/asca_sis.html).

The ASCA GIS has an energy range from 0.7 keV to 10 keV, an energy resolution of 8 percent at 5.9 keV, and a circular field of view with a diameter of 50 arcminutes (http://heasarc.gsfc.nasa.gov/docs/asca/asca_gis.html). Since our study is concerned with soft X-ray spectra, the ASCA SIS provides better energy resolution as well as a lower energy range than does the GIS. All of the data used in this study is from the ASCA SIS.

The raw information transmitted to the ground from the satellite is called the telemetry file. This file also contains "housekeeping" information about the observation period. The useful data from the telemetry file is converted into an event file which is "unfiltered" (i.e. it still contains any bad data from a "hot pixel" etc.). Finally, these unfiltered event files are passed through a program called xselect with uses a standard set of criteria to flag any bad data. The screened event files for the observations of NGC 4258, NGC 1097, and NGC 1068 were all obtained through anonymous ftp from the archive at the High Energy Astrophysics Archive Research Center (HEASARC) at NASA Goddard Space Flight Center (GSFC). GSFC also provides instrument response files as well as blank sky event files which are created in the same way. These blank sky observations were used to subtract background contributions from the AGN data before processing.

The observation of NGC 4258 lasted from 19:18:03 UTC on May 15, 1993 until 18:38:03

UTC on May 16, 1993. NGC 1068 was observed from 18:28:57 UTC July 24, 1993 until 16:40:57 UTC July 25, 1993. The utilized data for NGC 1097 is from 06:27:56 UTC January 12, 1994 until 01:50:03 UTC January 13, 1994.

3. Analysis

The analysis of the ASCA observations of NGC 4258, NGC 1097, and NGC 1068 involved iterative fittings with computer codes designed for X-ray data analysis. Initially we fit each spectrum with a NASA-developed code called xspec. Xspec obtains the best continuum fit given specific models and AGN parameters. The continuum models which we found most useful and which are described in section 1 are: power law (due to Compton scattering), blackbody, bremsstrahlung, and photoelectric absorption by hydrogen (termed "wabs" by xspec).

The power law model in xspec is given by $A(E) = K*(E/1\ keV)^{-\Gamma_p}$, where Γ_p is the photon index of the power law (unitless) and K is measured in units of photons/keV*cm^2*s at 1 keV (http://www.astro.columbia.edu/~karlfor/xray/xspec/node240.html). The blackbody spectrum model used by xspec is $A(E) = K*(8.0525)*(E^2de)/(T^4*(e^{(E/kt)}-1))$, where T is the temperature in keV and K is the ratio of source luminosity to squared distance to the source (http://www.astro.columbia.edu/~karlfor/xray/xspec/node197.html). The wabs model in xspec is given by $M(E) = e^{(-nH\sigma(E))}$, where H is the equivalent hydrogen column density in units of 10^{22} atoms/cm^2, and $\sigma(E)$ is the photoelectric cross-section (not including Thomson scattering) (http://www.astro.columbia.edu/ ~karlfor/xray/xspec/node258.html).

I attempted several types of continuum fits of NGC 4258, consisting of combinations of the above models, and found that the best fit continuum consisted of a wabs component multiplying both power law and blackbody models (i.e. wabs * (power law + blackbody)). The

best fit wabs component required a hydrogen column density of 0.326×10^{22} atoms/cm^2. The power law photon index (Γ_p) is 1.709 with a normalization of 9.7×10^{-2} photons/keV*cm^2*s. The best fit temperature for the blackbody (kT_{BB}) is 5.69×10^{-2} keV with a normalization of 2.036 photons/keV*cm^2*s. This model has a reduced chi squared (red. χ^2) of 0.881.

The best fit model which also includes discrete features is of the form: wabs * (power law + blackbody + Gaussians), with an H value of 0.167×10^{22} atoms/cm^2. Γ_p is 1.755 with a normalization of 3.3×10^{-2} photons/keV*cm^2*s., while kT_{BB} is 5.47×10^{-2} keV with a normalization of 0.384 photons/keV*cm^2*s (see Figure 1).

The additional discrete features are as follows:

Line Energy (keV)	Line Width (10^{-2})(keV)	K (photons/keV*cm^2*s)	Tentative Element Identification[3]
0.420	1.24	3.422	N L
0.589	1.89	0.422	O L
0.628	9.80	0.349	O K
1.010	8.08	1.97×10^{-2}	Na K or Fe L
2.383	52.76	8.28×10^{-2}	S K

The reduced χ^2 for this simulated spectrum fit is 0.559, which is better than the continuum fit alone, and is significantly better than the fit in which the normalizations of the Gaussian features are set to zero (see Figure 2).

---

[3]K-shell ions are those whose valence electrons lie in the n=1 shell. L-shell ions are those whose valence electrons lie in the n=2 shell.

I found that the best fit continuum for NGC 1097 also consisted of a wabs component multiplying a sum of power law and blackbody models (see above), with an H column density of 0.538×10^{22} atoms/cm^2. Γ_p is 2.285 with a normalization of 0.320 photons/keV*cm^2*s, and kT_{BB} is 0.1015 keV with a normalization of 0.113 photons/keV*cm^2*s. The reduced χ^2 is 0.819.

The best fit model for NGC 1097 including discrete features is of the form: wabs * (power law + blackbody + Gaussians), with an H value of 1.21×10^{13} atoms/cm^2. Γ_p is 1.184 with a normalization of 6.4×10^{-2} photons/keV*cm^2*s, while kT_{BB} is 5.15×10^{-2} keV with a normalization of 2.93×10^{-3} photons/keV*cm^2*s. The required discrete features are as follows:

Line Energy (keV)	Line Width (keV)	Normalization (10^{-2}) (photons/keV*cm^2*s)	Tentative Element Identification
0.7642	0.078	8.24	Fe L
1.050	0.102	3.24	Ne K
1.338	7.69×10^{-2}	1.62	Mg K
1.709	0.137	1.93	Al K
2.182	0.166	1.27	Si K
2.773	0.000	0.029	S K

This model has a reduced χ^2 of 0.747, which is a small improvement from the continuum only fit.

I found that the best fit continuum for NGC 1068 was also a wabs component multiplying both power law and blackbody models (see above). The best fit H has a value of 0.121×10^{22} atoms/cm^2, while Γ_p is 2.472 with a normalization of 0.265 photons/keV*cm^2*s. kT_{BB} is 0.1486 keV with a normalization of 3.930×10^{-2} photons/keV*cm^2*s. This model has a reduced χ^2 of 1.07.

The best fit model which also includes discrete features is of the form: wabs * (power law + blackbody + Gaussians). The best fit wabs component was a hydrogen abundance of zero atoms/cm^2. Γ_p is 1.689 with a normalization of 9.3×10^{-2} photons/keV*cm^2*s. kT_{BB} is 0.183 keV with a normalization of 1.93×10^{-2} photons/keV*cm^2*s. The additional discrete features are as follows:

Line Energy keV	Line Width (10^{-2}) keV	Normalization (10^{-2}) photons/keV*cm^2*s	Tentative Elemental Identification
0.7134	0.00	0.043	O K
0.9332	8.58	6.42	Ne K
1.891	9.04	1.61	Si K

This model has a reduced χ^2 of 0.93.

The values for the reduced χ^2 are good for our models which include discrete features, though not enormously better than we find with continuum only. If we find features produced by different, particular ion species (e.g. some species of iron), the ratios of the line fluxes can be used to constrain plasma densities (Liedahl *et. al.* 1992). With good energy resolution we could also find a measure of the temperature (T) at which the features are produced through an analysis of the line widths (due to "Doppler broadening"). We can also glean geometric information (specifically the density of emitters and distance from the ionizing source (R)) from modeling, which tells us the ionization level (ξ) which is equal to the total luminosity (L) divided by the density of emitters and the square of the distance from the ionizing source (i.e. $\xi=L/nR^2$) [where

ξ is measured in units of ergs*cm/s, L is measured in units of ergs/s, n is measured in units of cm^{-3}, and R is measured in units of cm]. Modeling also tells us at what temperature T an ion species is abundant. Unfortunately, blind fitting with Gaussians (although a useful first step in "feeling out" the discrete features of a spectrum) cannot easily account for every feature which ought to arise from a gas at a specific ξ and T. Thus, a complete and accurate interpretation of the Gaussian features is at best complicated and at worst (depending upon telescope resolution) *very* incomplete. With this limitation in mind, we choose to derive geometric information about the line-emitting gas via a method involving more detailed modeling.

Our method centers upon accounting for thermal instability which arises in photionized plasmas. Photoionization occurs when radiant energy detaches electrons from ions in the plasma. This is one of the main modes of energy transport within the highly ionized gases, along with collisional excitation by thermal electrons. These transport processes occur in order to keep the gas in thermal balance (a state in which heating processes exactly balance cooling processes within the gas).

Using a plasma modeling computer code named xstar1 (described in detail below) we simulate photoionization using the basic continuum data from the xspec fits. We then determine at which temperatures the gas is thermally stable. Thermal instability arises in these gases because the net cooling of the gas decreases with the an increase in temperature. The processes which cool the gas (e.g. electron capture) occur at specific temperatures where ions efficient in these processes are abundant. However, as the temperature rises the more efficient ions become outnumbered by those ions which are less efficient at cooling. Hence the gas becomes unstable. In order to conduct an analysis of the thermal stability of the photoionized plasma, we assume that

any discrete feature arises only at a temperature at which the gas is in thermal balance and where the gas is thermally stable. That is, if the gas cannot exist at a temperature where the feature is produced, we should not see the feature in the spectrum.

As an example of the process of accounting for thermal instability, the process we used to study NGC 4258 is described here. Our main tool is the xstar1 code which uses the parameters from the initial xspec data (i.e. the ionizing spectrum and total luminosity) fitting along with an assumed column density to iteratively derive the temperatures and ionization levels where the gas is in thermal balance. We can graphically display log(T) versus log(Ξ) (where $\Xi=\xi/4\pi KT$). This plot, which we call an "s-curve" shows the set of points where net heating processes equal net cooling processes (see Figure 3). The S-shaped doubling back denotes those temperatures at which the gas is thermally unstable. This instability generally coincides at temperatures where the lowest Fe L species are abundant (Hess *et. al.* 1997).

In order to fit the spectra we assumed that the line emission arises in stable (existing) gas. Since we found that some of the observed and identified species peak in abundance near the temperature range where the gas is unstable, we further supposed that the line emission arises at temperatures near the endpoints of the unstable range. From our calculated s-curve we selected appropriate candidate T and ξ for each AGN. These values were then used as input for another computer code (named x116n5), which is more elaborate version of xstar1. X116n5 calculates the line emission at the stable temperatures and produces line emission spectra additive tables, or "atables", which we then used as models in xspec.

The original data were then fit in xspec using the original continuum parameters along with one or more atables. Each atable represents line emission at a specific temperature and

might account for one or more discrete features seen within the AGN spectrum (see Figure 7). Once the best fit (see Figures 4-6) was achieved with one or more atables, we were able to calculate geometric information about the AGN. Specifically, the volume of the emitting plasma, the distance of the plasma from the ionizing source, and density of the emitters within the plasma can now be calculated. The results of these calculations and an analysis of them are summarized in the following section.

IV. Results/Conclusion

The results of the thermal instability analysis and subsequent refitting of the AGN spectra are presented in this section. Our geometric goals were to determine R (the distance of the emitting gas from the source of ionizing radiation) as well as V (the volume of the emitting gas) for each AGN. We assume that the emitting gas forms a thin partial shell around the central source of ionizing radiation with thickness ΔR and with a radius equal to R + the Schwarzchild radius (R_S), and subtending solid angle $\Delta\Omega$. The Schwarzchild radius is the minimum distance an object traveling at the speed of light must be from a black hole in order to escape its gravitational pull ($R_S = (3\times10^3)$*M cm).[4]

We also calculated the emission measure (EM) of the ionized gas. The EM is a measure of the amount of emitting material producing a group of spectral features. R was calculated for each AGN using the formula: $R = (L/n\xi)^{1/2}$ (where ξ is the ionization level determined from xstar1 modeling, L is the total source luminosity derived from xspec fits, and n is the column density of emitters which is reasonably assumed to be (1×10^{14}) cm^{-3}). The emission measure was calculated by using: $EM = (4\pi D^2)*(K)/(1\times10^{-14})$, where D is the distance to the AGN in cm and

[4] M is the mass of the black hole in units of solar masses.

K is the normalization of the line emission model as determined by xspec. The volume of the emitting gas (V) is calculated from EM through the relation $V \sim EM/n^2$. Since we assume that the line-emitting gas takes the form of a thin shell subtending a solid angle $\Delta\Omega$, $V = \Delta\Omega(R+R_S)^2\Delta R$.

The results for NGC 4258 are as follows:

log (T) (K)	log (ξ) (ergs*cm/s)	R (10^{12} cm)	EM (10^{50} cm^{-3})	V (10^{30} cm^3)	$\Delta\Omega\Delta R$ (10^8) cm
4.474	0.520	46.0	1.1×10^{14}	1.1×10^{6}	5.1
6.097	2.040	8.0	5.6×10^{7}	0.6	8.1×10^{-5}
7.390	2.600	4.2	6.3×10^{5}	6.3×10^{-3}	3.1×10^{-6}
8.026	3.040	2.5	5.2×10^{-1}	5.2×10^{-9}	6.6×10^{-12}

The total source luminosity of NGC 4258 is 6.97×10^{41} ergs/s, and it is approximately 7 Mpc away from us.

The results for NGC 1097 and NGC 1068 are as follows:

AGN	L (10^{43} ergs/s)	D (Mpc)	log (T) (K)	log (ξ) (ergs*cm/s)	R (10^{12} cm)	EM (10^{50} cm^{-3})	V (10^{30} cm^3)
NGC 1097	1.71	17	5.3	2.28	30	3.4×10^{6}	3.4×10^{-2}
NGC 1068	1.91	22	7.6	2.64	21	3.0×10^{-2}	3.0×10^{-10}

$\Delta\Omega\Delta R$ for NGC 1097 is 38 cm, while $\Delta\Omega\Delta R$ for NGC 1068 is 6.6×10^{-7} cm.

We find that the line-emitting plasmas are all located on the order of 10^{12} cm away from the source of photoionizing continuum near to the Schwarzchild radius of the black hole. This places this gas inside the BLR, since the accepted upper limit distance to the BLR is 10^{16} cm away from the nucleus. This is a very interesting result since it occurs in each of the three AGN that we studied. This suggests that ionized emitting plasma may always be present within the BLR. It also offers a possible explanation of time variability in AGN emission. Since both BLR and NLR are composed of many clouds, our line of sight to an ionized line-emitting region may be periodically obscured by the BLR and NLR clouds over time. Observational exploration of this possibility can be undertaken through a series of high resolution spectroscopic measurements with one of the newer X-ray observatories.

We found a wide range of volumes among the emitting shells at different temperatures. At high T and ξ the shells are relatively thin, and at lower T the shells tend to be more substantial. The low EMs of the thinner shells implies a strong emissivity on the part of the ions which make up the plasma since they contribute significant spectral components in spite of their relatively small numbers.

Although NGC 1097 (which produces astrophysical jets) and NGC 1068 (which exhibits maser activity in its outer regions) have nearly the same total luminosity, fitting the ASCA spectrum of NGC 1068 requires emitters with a much smaller emission measure. That is, the EM in NGC 1068 is approximately 100 million times less than that in NGC 1097. This suggests that the jet-emitting AGN undergo a significant amount of continuum reprocessing. It could also mean that the astrophysical jet in NGC 1097 is being powered by continuum energy trapped near the AGN core.

It is also interesting to note the difference in EM among the line-emitting regions in NGC 4258. The emitting region at log (T) = 4.474 K has an EM nearly 10^{15} times larger than the region at log (T) = 8.026 K. The regions which are closer to the ionizing source have considerably lower EM than do line-emitting regions further from the nucleus. Although the spatial gradients of temperature and ionization level are very large near the center of the AGN, we see that ions near the AGN core still emit strongly, producing significant signatures which reveal the structure of the inner regions.

A. Conclusion

We are very encouraged by our results. This study is the first of its kind (i.e. an attempt to map the inner structures of AGN using thermal instability analysis), and it produced reasonable and interesting results which may hold physical significance. From our results we can conclude that our method is capable of mapping the inner regions of AGN and other accretion powered systems. It holds the potential to be a very powerful tool when used along with observations of these objects at other wavelengths. Through a multi-wavelength study one could explore the morphologies of the galaxy beyond the AGN.

In the future, an exploration of the time variability of these AGN would be enlightening. By analyzing the changing spectrum over the course of a single observation and much longer periods (months or years) a better understanding of the geometry of these objects could be attained. The role of the BLR and NLR in obscuring the emission from the photoionized regions is of particular interest. Along with a study of time variability, a modeling which utilizes both higher and lower column densities would likely improve the accuracy of the calculations of the emitting plasma volumes. More accurate values for the volumes of the photoionized shells would

be possible with a modeling for which density is a free parameter since each line-emitting region could have a distinct value of n. This would also provide insight into the large variation in EM for these line-emitting regions.

Also helpful in the future would be the use of different elemental abundances within the models. This would alter the levels of ionization and therefore change the temperatures at which thermal balance occurs. Finally, three new telescope observatories (the Advanced X-ray Astrophysics Facility (AXAF) , ASTRO-E, and the X-ray Multimirror Mission (XMM)) all will employ spectroscopic instruments. AXAF will have a spatial resolution and energy resolution much greater than ASCA, and XMM is designed specifically for spectroscopy of distant objects. Discrete line emission will be very well resolved with these instruments and measures of luminosity should be much more accurate, all leading to a better description of the mysterious, distant, and unique objects known as AGN.

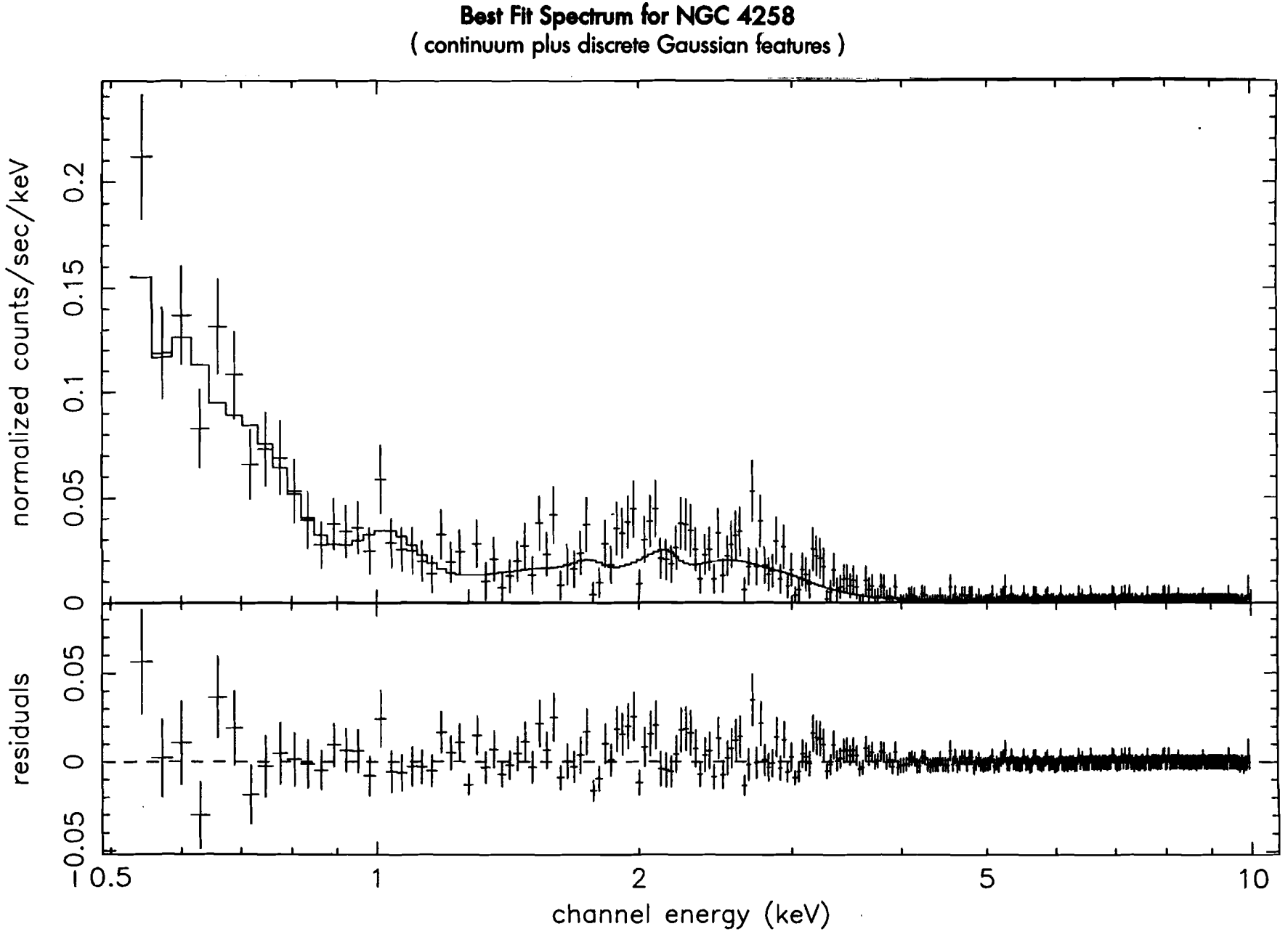

Figure 1: Best fit spectrum for NGC 4258 including continuum spectrum along with discrete Gaussian features. The top window displays the model and data. The bottom window displays the residual features above and below the model.

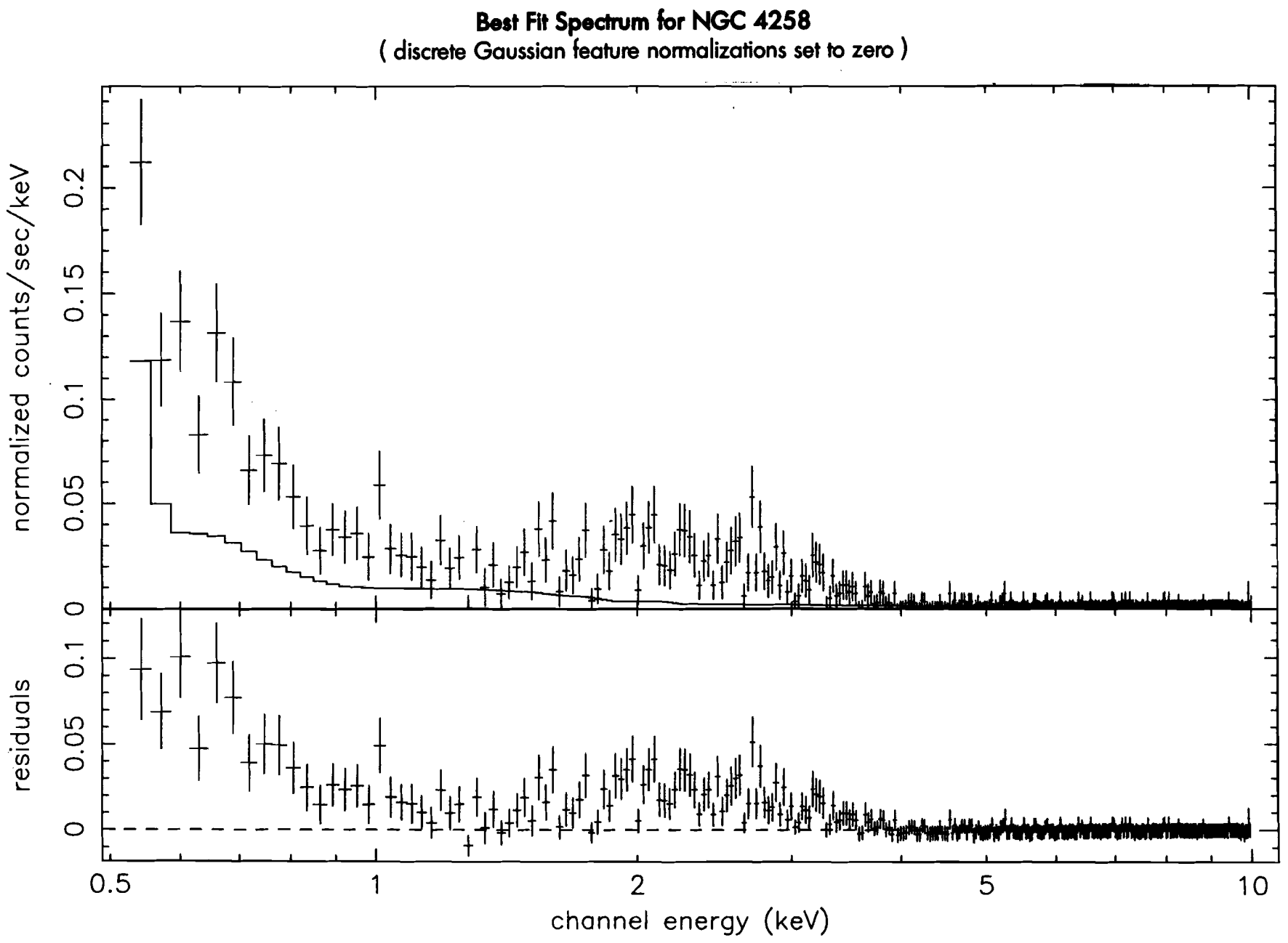

Figure 2: Best fit spectrum for NGC 4258 showing the continuum spectrum only (the normalizations of the discrete Gaussian features are set to zero).

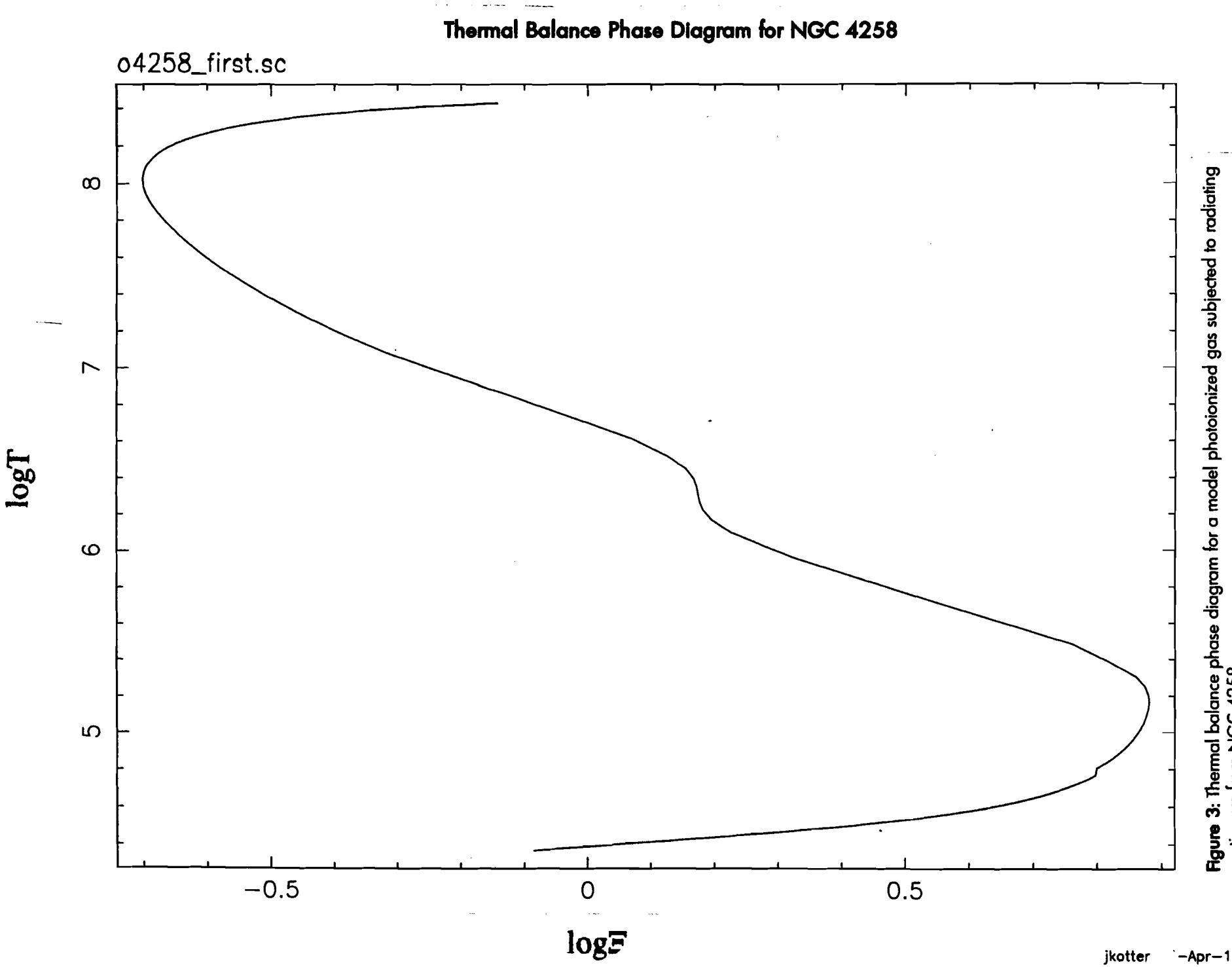

Figure 3: Thermal balance phase diagram for a model photoionized gas subjected to radiating continuum from NGC 4258.

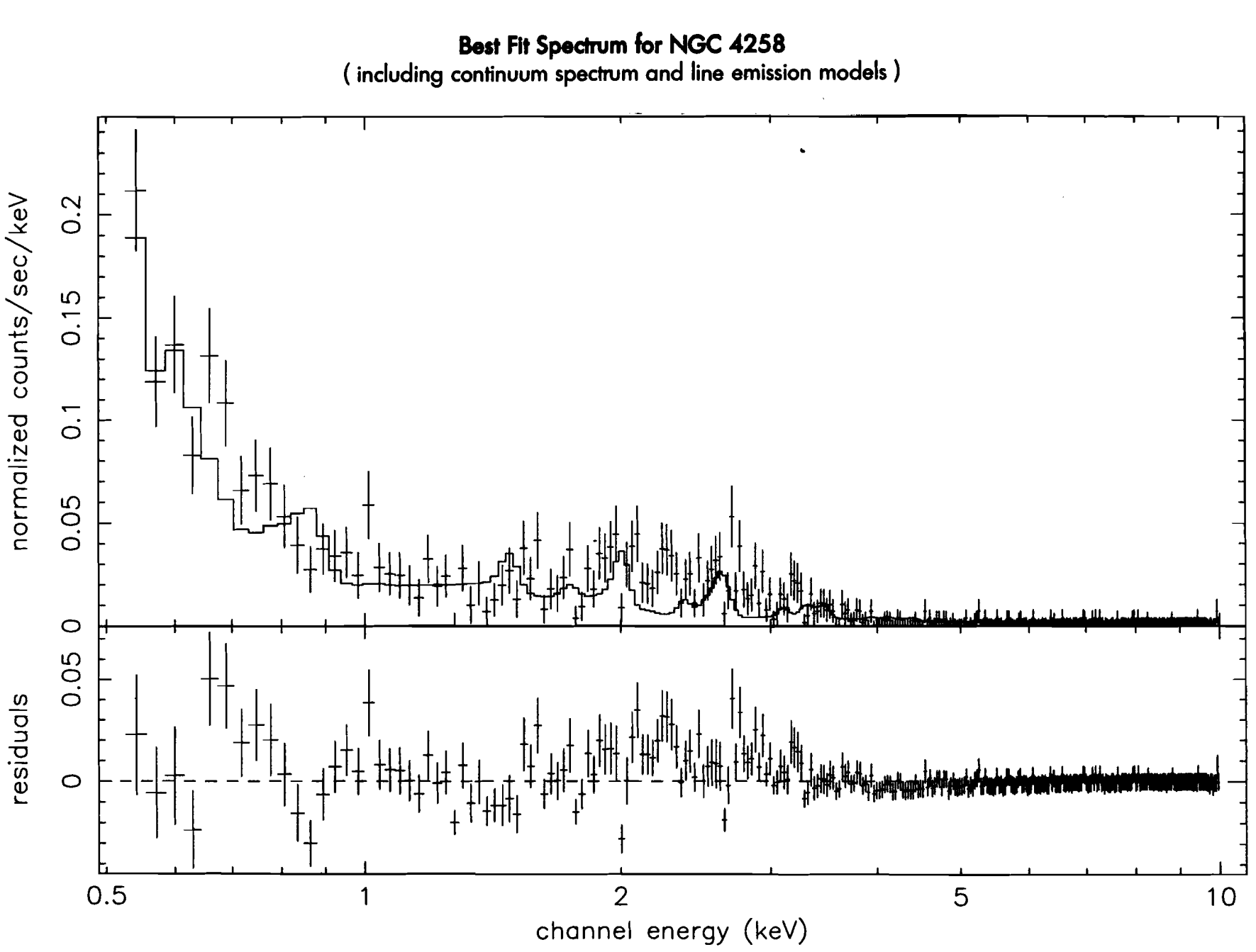

Figure 4: Best fit model for NGC 4258 including continuum spectrum and line emission models.

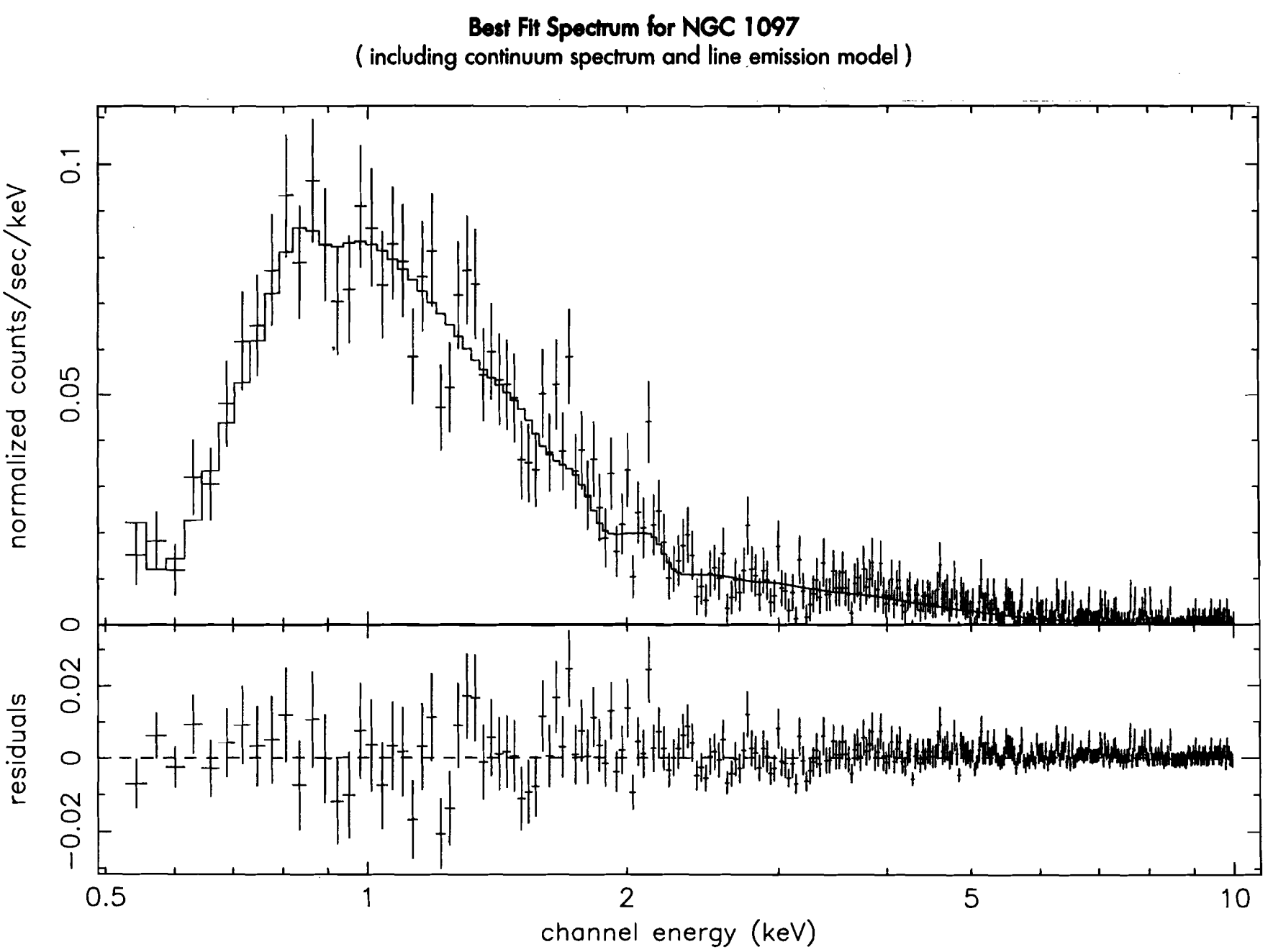

Figure 5: Best fit model for NGC 1097 including continuum spectrum and line emission models.

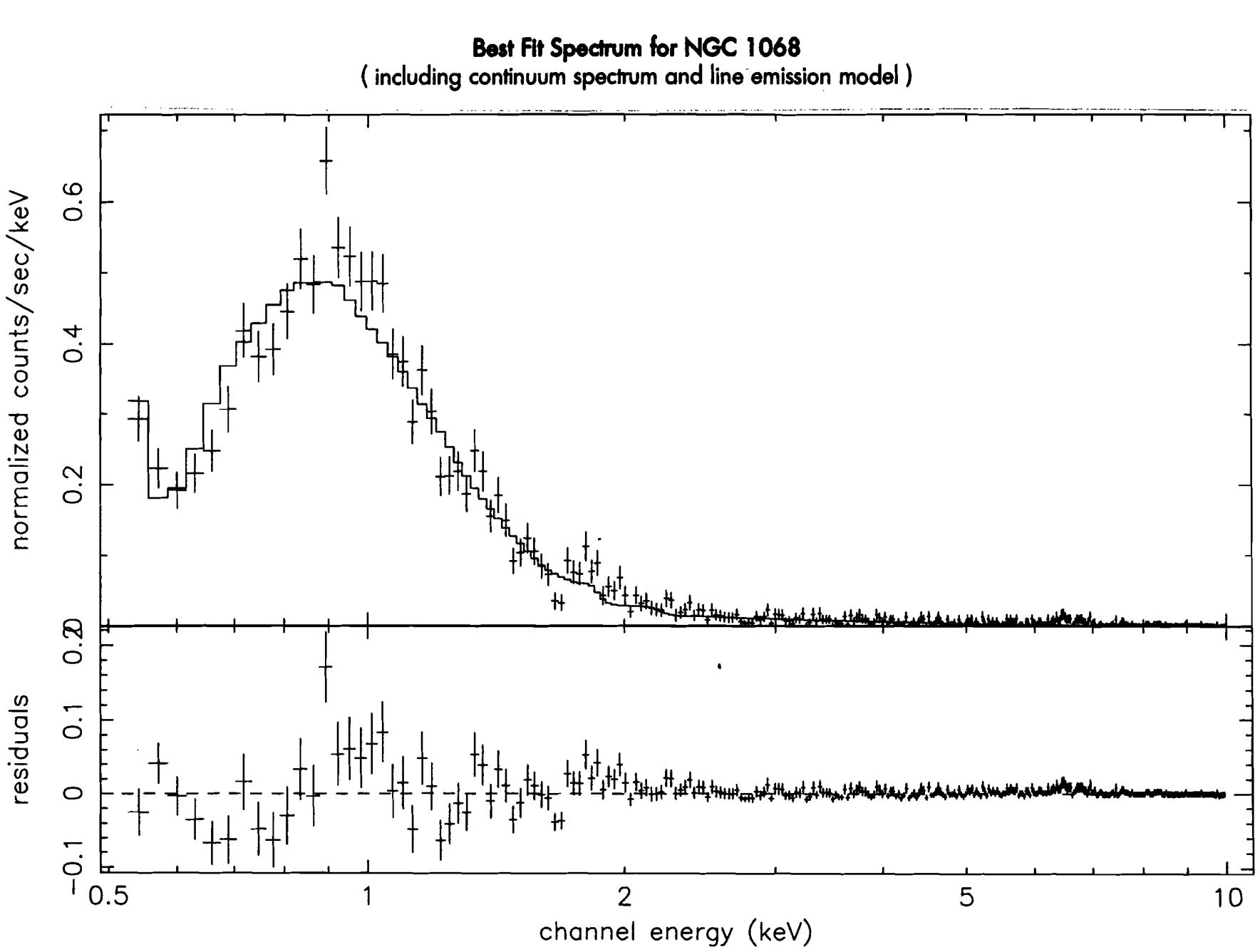

Figure 6: Best fit model for NGC 1068 including continuum spectrum and line emission models.

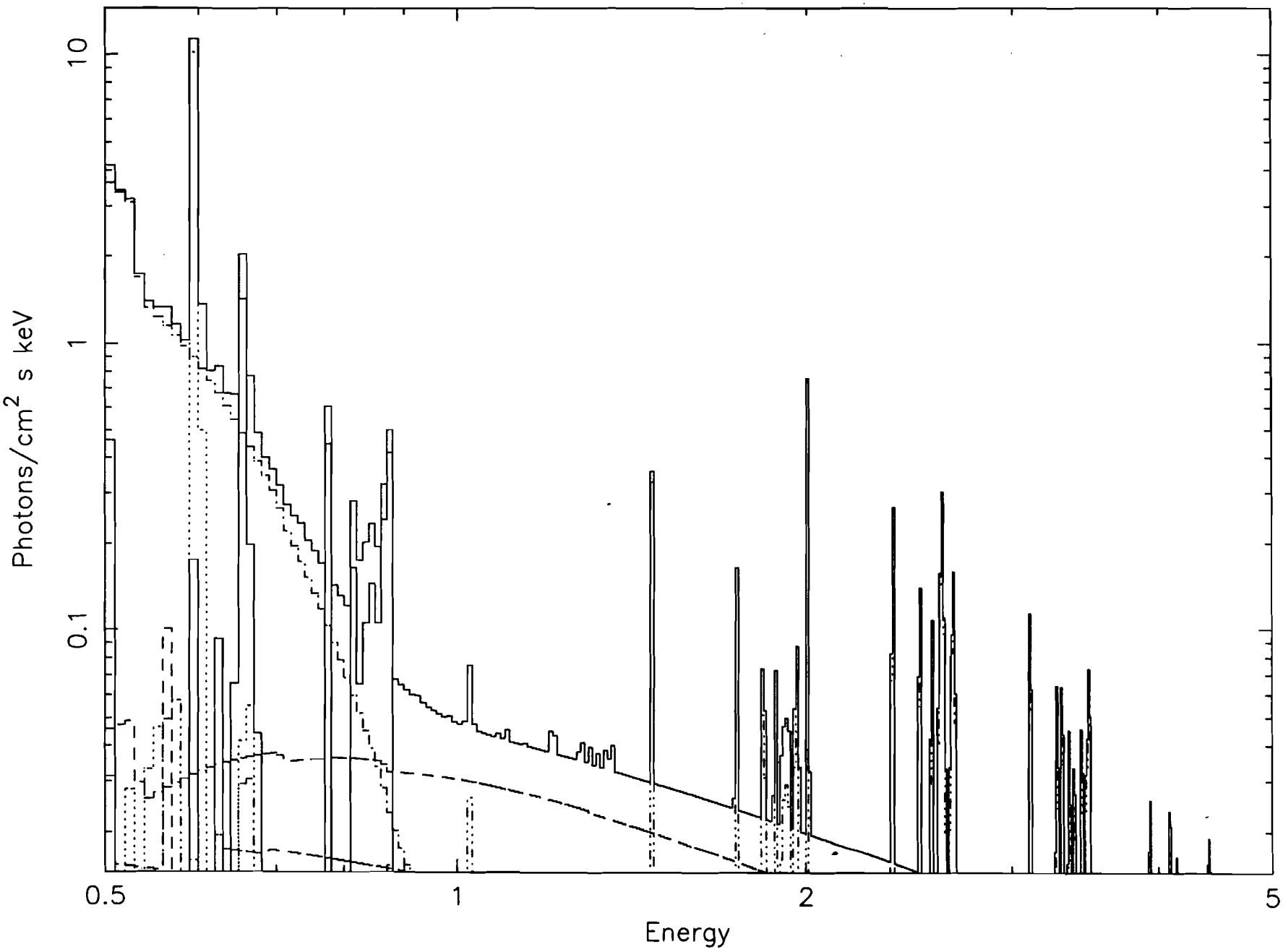

Figure 7: Best fit model for NGC 4258 including continuum spectrum and line emission models. The model is plotted to display the effect of the line emission.

References

Burbridge, E.M. , & Burbridge, G. 1997, ApJ, 477, L13

Hess, C. J., *et. al.*,1997, ApJ, 478, 94

http://heasarc.gsfc.nasa.gov

http://www.astro.columbia.edu

Liedahl, D. A., *et. al.*, 1992, ApJ, 391, 306

Makishima, K., *et. al.*, 1994, PASJ, 46, L77

Marshall F. E., *et. al.*, 1993, ApJ, 405, 168

Netzer, H., 1993, ApJ, 411, 594

Perez-Olea, D. E., & Colina L., 1996, ApJ, 468, 191

Peterson, B. M., An Introduction to Active Galactic Nuclei, Cambridge University Press: Cambridge, 1997.

Storchi-Bergmann, T., Baldwin, J. A., & Wilson, A. S., 1993, ApJ, 410, L11

Telesco, C.M., & Gatley, I., 1981, ApJ, 247, L11

Ueno, S., *et. al.*, 1994, PASJ, 46, L71

Zeilik, M., Gregory, S. A., & Smith, E. V. P., Introductory Astronomy and Astrophysics, Saunders College Publishing: Fort Worth, 1992.